fractal and fractional

MDPI

Article

Power Quality Conditioners-Based Fractional-Order PID Controllers Using Hybrid Jellyfish Search and Particle Swarm Algorithm for Power Quality Enhancement

Abdallah Aldosary

Computer Engineering Department, College of Engineering, Prince Sattam bin Abdulaziz University, Wadi Addwasir 11991, Saudi Arabia; ab.aldosary@psau.edu.sa

Abstract: Power quality (PQ) is a major issue in today's electrical system that affects both utilities and customers. The proliferation of power electronics devices, smart grid technology, and renewable energy sources (RES) have all contributed to the emergence of PQ concerns in today's power system. The Unified Power Quality Conditioner (UPQC) is a versatile tool that can be used to fix distribution grid issues caused by irregular voltage, current, or frequency. Several tuning parameters, however, restrict the effectiveness of the Fractional-Order Proportional Integral Derivative (FOPID) control technique, which is proposed to improve UPQC performance. To move beyond these restrictions and find the optimal solution for the FOPID controller problem, a hybrid optimization strategy called the Hybrid Jellyfish Search Optimizer and Particle Swarm Optimizer (HJSPSO) is employed. To meet the load requirement during PQ issue periods, the suggested model incorporates a renewable energy source into the grid system. Whether the load is linear or non-linear, the design maintains PQ problems to a minimum. Furthermore, the FOPID control technique is compared with other controllers. Results show that grid-connected RES systems using the proposed FOPID control approach for UPQC have fewer PQ problems. The presented UPQC with HJSPSO strategy significantly outperformed, with the shortest computing time of 127.474 s and an objective function value of 1.423.

Keywords: fractional-order controllers; disturbances; optimization; power quality; total harmonic distortion; unified power conditioners

Citation: Aldosary, A. Power Quality Conditioners-Based Fractional-Order PID Controllers Using Hybrid Jellyfish Search and Particle Swarm Algorithm for Power Quality Enhancement. *Fractal Fract.* **2024**, *8*, 140. https://doi.org/10.3390/fractalfract8030140

Academic Editors: Chendrayan Dineshkumar, Velusamy Vijayakumar and Norbert Herencsar

Received: 30 January 2024
Revised: 20 February 2024
Accepted: 21 February 2024
Published: 28 February 2024

Correction Statement: This article has been republished with a minor change. The change does not affect the scientific content of the article and further details are available within the backmatter of the website version of this article.

1. Introduction

The incorporation of renewable sources, such as photovoltaic (PV) systems, into microgrids (μGs) has gained significant attention as a means to promote sustainable and reliable energy generation [1]. However, the intermittent and fluctuating nature of renewables can present power quality (PQ) challenges, including voltage fluctuations, harmonics, and reactive power imbalances [2]. To address these issues and ensure the efficient and reliable operation of μGs, advanced control strategies for PQ enhancement are essential [3,4].

There is a growing need for environmentally friendly energy sources due to the fact that the demand for energy has been on the rise, which has increased emissions of greenhouse gases [5]. Renewable energy sources (RES) have emerged as a promising solution, offering environmentally friendly power generation without harmful emissions. Among the various RES technologies, PV systems and wind systems have gained substantial attention due to their widespread adoption. Integrating different types of distributed generation (DG) units into standalone μGs allows for the effective utilization of their complementary attributes. However, the intermittent nature of RES and load fluctuations, such as non-linear loads, unbalanced loads, and critical loads, introduces PQ issues and stability challenges in standalone μGs [6,7].

PQ issues, including disturbances, sags, harmonics, and swells, arise due to the intermittent environmental changes affecting RES and the dynamic nature of loads [8]. Addressing these issues is crucial for enhancing the dependability and stability of standalone

microgrid systems [8,9]. Flexible Alternating Current Transmission Systems (FACTS) devices, such as filters and power quality custom devices, are commonly employed to mitigate PQ problems in standalone μGs. These devices include series and shunt compensators, which are integrated into μGs to regulate and correct voltage problems [10,11]. However, managing compensators effectively can be challenging, as they rely on controller output signals. Diverse control approaches, such as Fractional-Order Proportional Integral Derivative (FOPID) controllers and Fuzzy Logic Controllers (FLC), have been employed to address power quality issues.

In this work, a novel, hybrid optimization built FOPID controller for a unified power quality conditioner (UPQC) is proposed to enhance PQ in integrated microgrid systems. By combining the jellyfish optimizer (JO) and the particle swarm optimizer (PSO), a hybrid jellyfish search optimizer and particle swarm optimizer (HJSPSO) algorithm is employed. This hybrid approach reduces decision-making time and enables researchers to focus on data analysis. The principal goal of this work is to improve PQ in a hybrid RES-grid-connected non-linear distribution system using the proposed FOPID controllers for UPQCs.

1.1. Related Works in the Literature

Several studies have been conducted to address PQ issues in integrated systems, particularly in the context of RES and μGs [4,12]. Researchers have explored various techniques and control strategies to boost the performance and stability of those schemes [13,14]. Enhancing PQ in a system is a crucial task within the power system domain. Several models have been introduced to mitigate PQ issues [15], and recent developments in these areas are reviewed as follows:

In ref. [16], a hybrid active power filter (APF) was developed to improve PQ. The adaptive ANFIS approach was employed to evaluate the PQ performance of the UPQC scheme. Although UPQC devices have some drawbacks, such as swell and sag, these issues were minimized by utilizing sophisticated hybrid techniques. In ref. [17], a FOPID controller called a distributed power flow controller (DPFC) was introduced, which serves as the drive controller. It was tuned using the black widow optimization technique. While this controller compensates for voltage and harmonics, it may not be capable of detecting power system issues. In ref. [18], an adaptive Bald Eagle optimization algorithm (ABE-OA)-based FOPID controller integrated with UPQC was proposed to reduce total harmonic distortion (THD) and tackle problems such as swell, sag, non-linear load, disturbances, and unbalanced load. Although this strategy is effective, more advanced hybrid algorithms can be employed for improved control strategies. In ref. [19], the synchronous reference frame-power angle control (SRF-PAC) strategy was developed, which divides the reactive power load between two inverters using the PI methodology. This approach's performance was assessed under different operating circumstances, incorporating PV irradiation variation, voltage fluctuation, and voltage harmonic injection. However, the system cost is high. In ref. [20], the utilization of a Fractional-Order Proportional Integral (FOPI) and Fractional-Order Fuzzy Logic (FOFL) control strategy for the UPQC scheme was proposed. By integrating these tools through an enhanced control system, the aim is to enhance the system's dependability, achieve a rapid dynamical response, and reduce the THD to improve the overall PQ. In ref. [21], a wind energy system coupled with UPQC to enhance the quality of energy output was developed. An adaptive Proportional-Integral (PI) controller was used for both serial and shunt-based APFs, enabling the Park control mechanism. Although the controller performs well, system stability is a concern. In ref. [22], a multi-converter, unified fuzzy-based PQ controller for enhancing PQ was proposed. The fuzzy gradual conductance approach was used to identify the peak power source. While this fuzzy-based technology improved wind energy infrastructure to some extent, there is still room for further improvement. In ref. [23], it was proposed that the implementation of a UPQC serves the purpose of improving the performing of the microgrid and resolving PQ concerns associated with the sensitive loads. In ref. [24], the PV-UPQC scheme was proposed, which was tested using a reinforcement learning algorithm and an adaptive

neuro-fuzzy controller. The fuzzy model enhances system efficiency by assisting in generating reference currents and determining system parameters using linguistic rules. However, it is not suitable for grid-connected renewable energy systems. In ref. [25], an improved FOPID controller with a GS algorithm to demonstrate a method for Dynamic Voltage Restorer (DVR) was employed. This approach successfully addressed various PQ issues, including fault compensation, voltage regulation, sag, THD reduction, and swell. However, it has a complex structure. In ref. [26], a PQ strategy was proposed to mitigate light flickers, voltage stability, and harmonics in the utility of large-scale LED lighting networks. To address these PQ concerns comprehensively, a transformerless UPQC (TL-UPQC) and its control system are introduced. The PI controller's gain values are determined through the utilization of an extended Bald Eagle search (EBES) optimizer. In ref. [27], the Cuckoo optimization method was introduced, which adjusts the parameters of the PI control strategy in shunt controllers to reduce THD and enhance PQ. Instantaneous PQ theory was employed to produce reference signals essential for shunt and series controllers, along with DQ-conversion evaluation. However, this method is not suitable for the unity power factor mode of operation. In ref. [28], a cutting-edge, three-phase, multi-objective unified power quality conditioner (MO-UPQC) that integrates interfaces for PV panels and battery energy storage was proposed. The MO-UPQC effectively addresses PQ issues in both voltage (at the load side) and current (at the grid side). Additionally, it facilitates power injection into the grid (from PV panels or batteries) and battery charging (from PV panels or the grid). In ref. [29], a groundbreaking algorithm that employs variable phase angle control optimized using the JAYA optimization technique (JAYA is a Sanskrit word signifying victory or triumph) was proposed. The primary goal was to identify the optimal power angle that minimizes the volt-ampere (VA) loading of the unified power quality conditioner (UPQC) without diminishing its compensation capabilities. In ref. [30], optimizing UPQC control strategies were focused on, particularly in unbalanced and distorted weak grid conditions. Additionally, UPQC performance under unbalanced and non-linear harmonic loads was crucial for maintaining desirable power quality.

The literature mentioned above primarily focuses on PQ issues in a single microgrid operating in grid-connected mode. However, these techniques have limitations, such as complex design, poor reliability [12], the need for improvement [13,15,16], complex structure [14], inadequate performance due to unstable voltage and current supply [17,18,20], and high cost [19,21]. To address these problems and enhance system performance in the distribution system, integration with Flexible AC Transmission Systems (FACTS) is proposed. This integration aims to mitigate power supply problems and ensure an adequate power supply. Consequently, the proposed design introduces a novel control mechanism for operating the FACTS device in a hybrid renewable system under various PQ issue scenarios.

1.2. Contributions and Organization

The main contribution of this research can be briefed as follows:

- A hybrid RES-based grid with a load model, where UPQC is connected to manage PQ.
- The FOPID controller is utilized to generate pulse signals for the switches of the UPQC compensator by comparing the actual and reference values.
- The parameters of the FOPID controller are regulated by utilizing the employed HJSPSO optimization algorithm.
- The performing of the proposed model is evaluated under numerous PQ conditions, including sags, harmonics, interruptions, and swells.
- A comparative analysis between other controllers and optimization techniques is implemented.

The manuscript is organized as follows: Section 2 outlines the general layout and procedure of the presented work. Section 3 introduces the control strategy of the presented UPQC. The problem formulated and the hybrid algorithm used are presented in Section 4.

The evaluation of performance of the suggested model is introduced in Section 5. Lastly, Section 6 introduces the overall conclusions.

2. System Investigation

Figure 1 illustrates the proposed configuration, which includes a PV plant with a three-phase PWM inverter, a wind system, and a network connection to non-linear loads of 1500 kW which operates with a power factor of 0.7 lagging. Step-up transformers are employed with both the PV and wind systems to coordinate them through the network with a three-winding transformer. The PV system has a size of 750 kilowatts and is connected to a 1000 kVA, 0.6/22 kV, 50 Hz step-up transformer (T_2). The DFIG wind turbine has a size of 0.5 MW and is linked to a 0.75 MVA, 0.6/22 kV, 50 Hz step-up transformer (T_1).

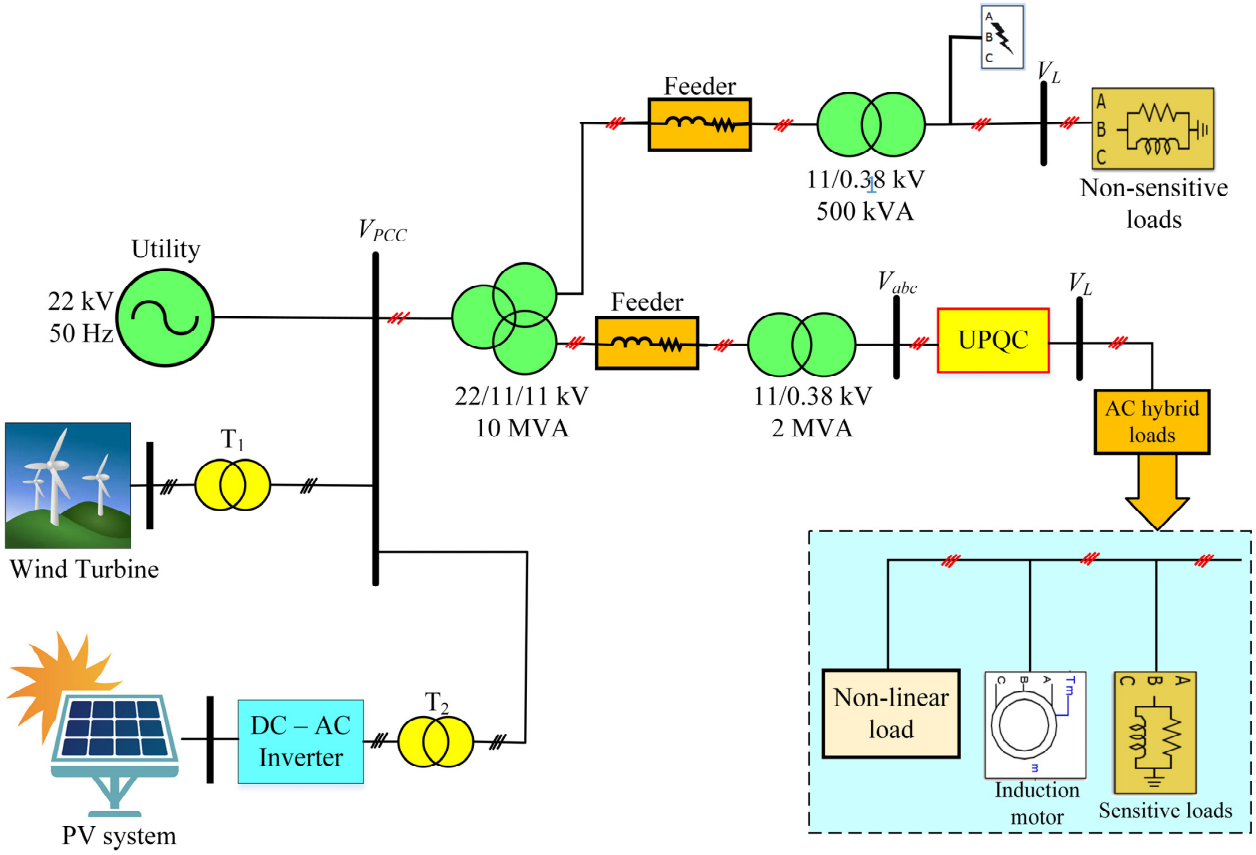

Figure 1. The system investigated in this study.

2.1. PV Plant

The power output of a PV plant can be assessed utilizing the following equations [31,32]:

$$P_{PV} = \eta_g N_{PV} A_m G_i \tag{1}$$

In Equation (1), N_{PV} represents the number of PV modules, and η_g denotes the generation efficiency. A_m and G_i stand to the area per module (in square meters) and the whole irradiant on the angled plane (in watts per square meter), respectively [33]. The PV efficiency, η_g, can be estimated utilizing the following equation:

$$\eta_g = \eta_r \eta_{pt} [1 - \beta_t (T_c - T_r)] \tag{2}$$

In Equation (2), η_r represents the efficiency of the PV reference, and η_{pt} represents the efficiency of the tracked power equipment when MPPT is utilized (both assumed to be

equal to 1). T_r and T_c represent the temperatures of the reference and PV cells, respectively, measured in degrees Celsius. β_t signifies the efficiency temperature parameter.

2.2. Wind System

The mechanical power can be estimated using Equation (3), expressed as follows [34]:

$$P_w = \frac{1}{2}\rho A C_p(\lambda, \beta) V_w^3 \tag{3}$$

In Equation (3), ρ signifies the air density measured in kilograms per cubic meter, A represents the rotor displacement point in square meters, C_p represents the power coefficient (ranging from 0.250 to 0.450) depending on λ (lambda) and the screwed angle β (beta), and V_w represents the wind velocity in meters per second.

3. Unified Power Quality Conditioner

3.1. Configuration of UPQC

The UPQC consists of two interconnected power electronic converters using a single AC wire [35–37]. Power electronic devices for power conditioning play a crucial role in improving the efficiency of the power grid and addressing PQ concerns, as depicted in Figure 2. The UPQC-PQ can effectively handle PQ concerns, like harmonics, flickers, imbalance, sag, and swell. The UPQC-PQ primarily utilizes voltage source inverters (VSIs), including series and shunt APFs, along with a DC connection capacitor. The DC-link capacitor is a critical component required to regulate the voltage between the two filters. The power system of the UPQC-PQ could be split up into several distinct parts, including active filters for series and shunt circuits, as well as power generation and supply systems [38,39].

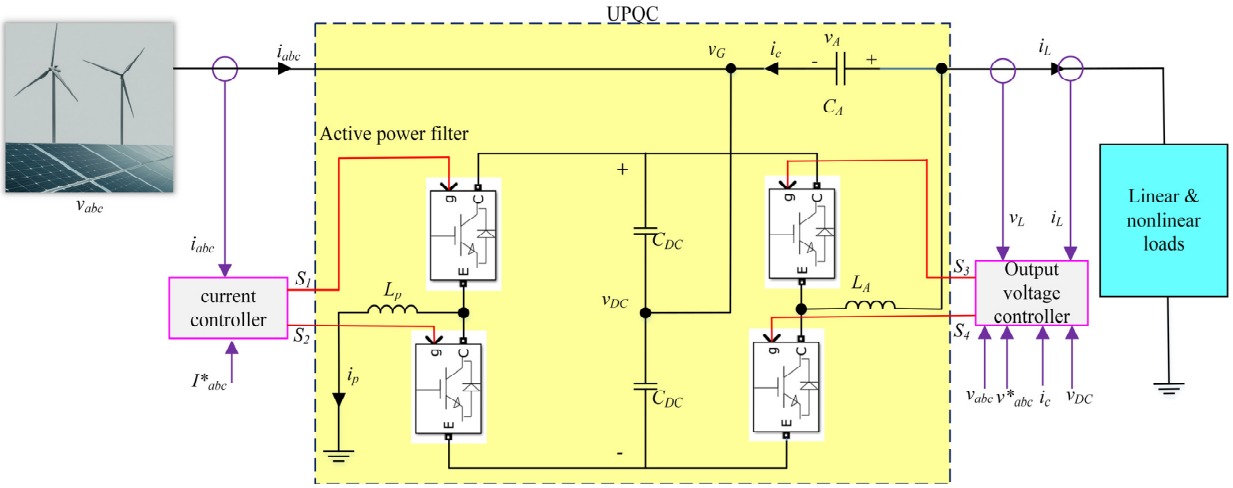

Figure 2. The presented UPQC scheme.

The behavior of the power supply system can be mathematically represented by Kirchhoff's law, as shown in Equations (4) and (5):

$$V^{if} = e^i - L^s \frac{di_s}{dt} - R^s I^s - V^{ih} \tag{4}$$

$$I^{is} = I^{iL} - I^{ih} \tag{5}$$

In the above equations, I^{ih} denotes the output current of the APF, I^{iL} and I^{is} represent the load and the line currents, respectively, V^{ih} denotes the output voltage of the series active filter, e^i is the source voltage, L^s represents the inductor of the transmission line (TL), R^s represents the resistor of the TL, and the subscript i stands to the phases in a network (a,

b, and c phases). The series and shunt active filters in the UPQC-PQ scheme regulate the source current and load voltage, respectively, to address PQ issues.

During PQ disturbances, the active filters provide the necessary voltage and current. The load and source currents are often denoted as $I(ch)$ and $I(s)$, respectively. $I(f)$ represents the injecting current of the APF, while $V(c)$ denotes the injecting voltage of the APF. The reference load voltage is indicated by $V(ch)$, and the fluctuation in the source voltage factor can be signified by the symbol k, while the power factor can be denoted as $\cos(\varphi(n))$. Equation (6) shows the percentage change between the source and the reference voltages. When the system experiences overvoltage VG, the series inverter injects the negative voltage $V(s)$ into the network to mitigate it.

$$V(c) = V(ch) - V(s) = -kV(ch) < 0 \tag{6}$$

To find the solution to the previous equation, one can use Equation (7).

$$k = \frac{V(s) - V(ch)}{V(ch)} \tag{7}$$

In UPQC-PQ models, losses cannot be considered. The active power and load power requirements are compared to the input power requirements at the V_{abc}. Equation (8) illustrates the *abc* side current:

$$I(f) = \frac{I(ch)}{1+k} cos\varphi(n) \tag{8}$$

The UPQC dc link voltage can noticeably maintain its reference value during transient events caused by load connecting/disconnecting or supply voltage sag/swell, even while the average DC link voltage remains constant in steady state. The size of the load voltage changes because the series injecting voltage cannot stay constant during such transients due to the significant DC link voltage fluctuations.

Under normal operating conditions, the voltage at the common bus prior to a voltage sag ($V_{Pre\text{-}sag}$) and the line current (I_{abc}) can be determined using Kirchhoff's voltage law (KVL) applied to a typical DVR system, as shown in Equations (9) and (10):

$$V_{pre-sag} = V_{abc} - I_{abc} Z_{abc} \tag{9}$$

$$I_{abc} = I_1 + I_2 = \frac{V_{pre-sag}}{Z_{tot} + Z_{L2}} + \frac{V_{pre-sag}}{Z_{tot} + Z_{L1}} \tag{10}$$

when a fault (F) occurs on the first feeder, a high current (I_{fault}) flows through it. Consequently, the voltage at the common bus during the voltage sag (V_{sag}) can be calculated using Equations (11) and (12):

$$V_{sag} = V_{abc} - I_{fault} Z_{abc} \tag{11}$$

$$I_{fault} = I_1 + I_2 = \frac{V_{sag}}{Z_{tot}} + \frac{V_{sag}}{Z_{tot} + Z_{L1}} \tag{12}$$

Therefore, the phasor diagram shown in Figure 3 illustrates the injected voltage (V_j) during the voltage sag condition. The magnitude and angle of the injected voltage are determined by Equations (13) and (14):

$$|V_j| = \sqrt{V_{L2}^2 + V_{abc}^2 - 2V_{L2}V_{abc} cos(\varnothing_{L2} - \varnothing_{abc})} \tag{13}$$

$$\varnothing_j = \tan^{-1}\left(\frac{V_{L2}\sin\varnothing_L - V_{abc}\sin\varnothing_{abc}}{V_{L2}\cos\varnothing_L - V_{abc}\cos\varnothing_{abc}}\right) \tag{14}$$

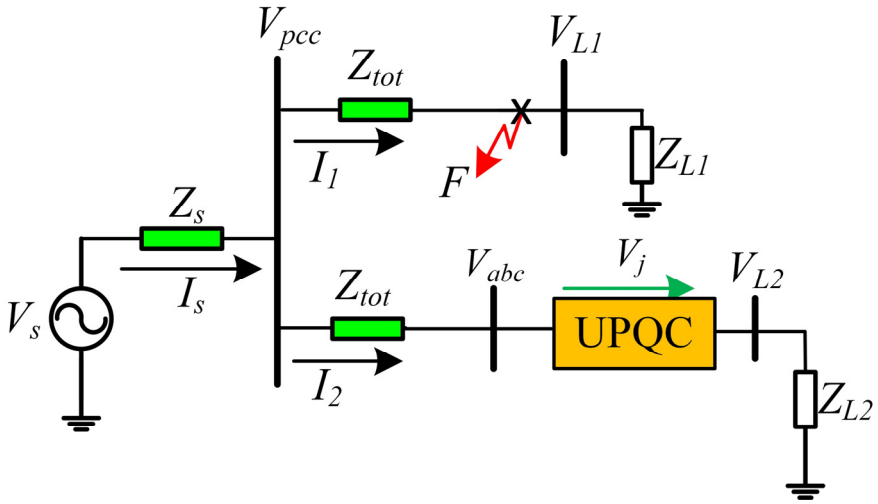

Figure 3. Thevenin equivalent circuit of UPQC scheme.

This architectural design employs a series converter that injects voltage into the grid during voltage sags. This injected voltage is synchronized with the grid voltage. In the event of a voltage swell, the injected voltage is shifted out of phase with the grid voltage.

Figure 4 illustrates the phasor diagram under normal conditions, voltage swell, and voltage sag. During a voltage swell, the phasors represent the grid voltage (v'_{abc}), grid current (v'_L), injected voltage (v'_A), output current (i'_{abc}), shunt current (i'_L), and shunt current (i'_P). During a voltage sag, the corresponding phasors are v''_{abc}, v''_L, v''_A, i''_{abc}, i''_L, and i''_P. The system operates in three modes:

(a) Reactive power mode: The UPQC functions as a reactive power compensator.
(b) Energy absorption mode: The UPQC absorbs energy through the series converter to balance the additional power.
(c) Energy supply mode: The UPQC uses the series converter to supply energy and restore lost power.

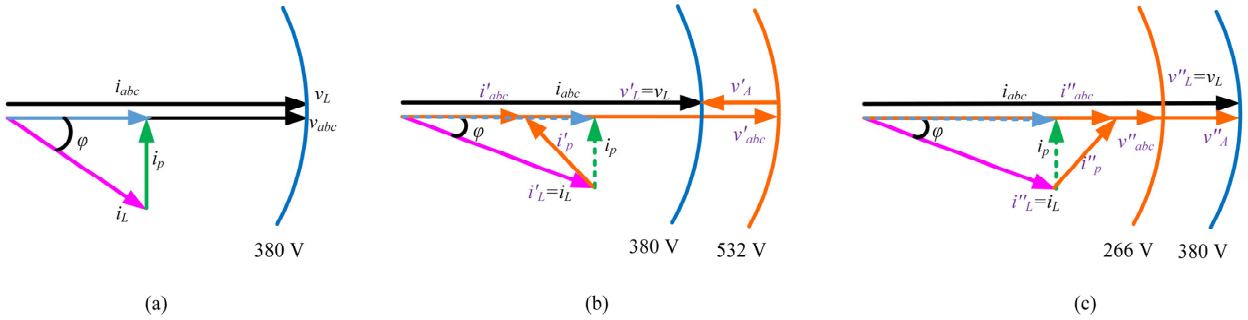

Figure 4. Phasor diagram of UPQC scheme: (**a**) normal operation, (**b**) swell mode, and (**c**) sag mode.

In steady-state operation, the shunt converter provides the active power required by the series converter in modes (b) and (c).

3.2. Control Strategy of UPQC

The controller of the UPQC's APF is depicted clearly in Figure 5.

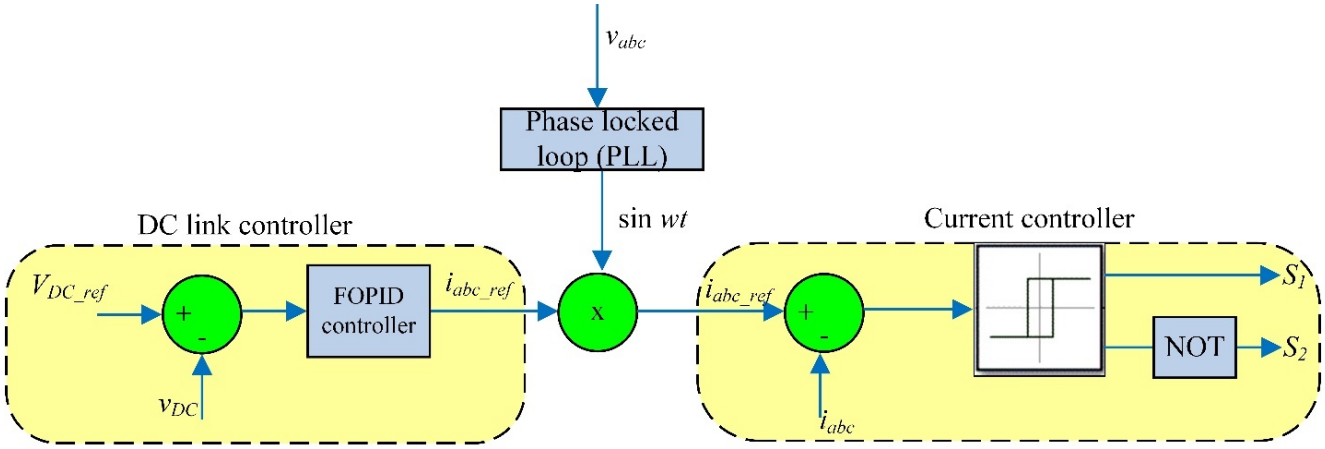

Figure 5. Control circuit of the UPQC scheme.

Two controllers, one for voltage and one for current, form the shunt APF. A FOPID controller modifies the DC link voltage in the external voltage control loop. The internal control loop uses hysteresis control to compare the input current to a reference signal that is created by the external loop and a phase-locked loop (PLL). The internal loop uses this reference signal to determine the input current.

Switching conditions for S_1 = on and S_2 = off are as follows: when the lower band of the inductor current can be retrieved, the hysteresis control changes the operating styles of the switches, turning S_1 on while S_2 is off, allowing the inductor current time to start charging. The switching criteria can be expressed as:

$$i_P(t) \leq i_P^*(t) - \frac{\Delta I_p}{2} \tag{15}$$

where ΔI_p signifies the hysteresis zone in the reactor current, and $i_P^*(t)$ is the reference reactor current.

Switching criteria for S_1 = off and S_2 = on are as follows: upon attainment of the upper band of the inductor current, the controller activates to adjust the operational conditions of the switches, turning S_1 off while S_2 is on, enabling the discharge of the reactor current. The switching specifications can be expressed as:

$$i_P(t) \geq i_P^*(t) + \frac{\Delta I_p}{2} \tag{16}$$

Figure 3 shows that the APF scheme and the UPQC system operate in parallel. The network ripple and reactor currents are equivalent under the assumption of a constant load current. As a result, it is possible to create a reference signal for the grid current that can be compared to the real network current. The following is another way to rewrite Equations (15) and (16) for the two switches cases:

$$i_{abc}(t) \leq i_{abc}^*(t) - \frac{\Delta I_{abc}}{2},\ S_1 = \text{on and } S_2 = \text{off} \tag{17}$$

$$i_{abc}(t) \geq i_{abc}^*(t) + \frac{\Delta I_{abc}}{2},\ S_1 = \text{on and } S_2 = \text{off} \tag{18}$$

Here, ΔI_{abc} represents the hysteresis ripple band of the reactor current, and $i_{abc}^*(t)$ represents the reference network current.

Passive mechanism voltages and currents can be predicted using the switching trajectory. Based on these predictions, the inverter's switching decisions (gate signals) are timed correctly. This proactive strategy guarantees a quick and adaptable reaction to any

outside disturbances. For the basic HBVSI topology, the following switching requirements were determined:

Switching criteria for S_3 = on and S_4 = off are given as

$$v_A(t) - v_{A,min} - \left[\frac{k_A}{\frac{v_{DC}}{2} - v_A(t)}\right] i_C^2(t) \leq 0 \tag{19}$$

$$i_C(t) \leq 0 \tag{20}$$

Switching criteria for S_3 = off and S_4 = on are given as

$$v_A(t) - v_{A,max} + \left[\frac{k_A}{\frac{v_{DC}}{2} + v_A(t)}\right] i_C^2(t) \geq 0 \tag{21}$$

$$i_C(t) \geq 0 \tag{22}$$

Here, k_A denotes a constant value defined as $k_A = \frac{L_A}{2C_A}$. The values $v_{A,min}$ and $v_{A,max}$ denote the minimum and maximum boundaries of the reference signal, respectively. The term ΔV corresponds to the hysteresis voltage ripple.

$$v_{A,min} = v_A^*(t) - \Delta V \tag{23}$$

$$v_{A,max} = v_A^*(t) + \Delta V \tag{24}$$

The control target of the UPQC is to keep a constant value of the load voltage (v_L). Therefore, the reference signal can be modified to be associated with Equation (4) as follows:

$$v_A^*(t) = v_L^*(t) - v_{abc}(t) \tag{25}$$

where $v_O^*(t)$ represents the reference load voltage. Thus, the switch criteria are re-obtained as follows:

Switching criteria for S_3 = on and S_4 = off:

$$v_L(t) - v_{L,min} - \left[\frac{k_A}{\frac{v_{DC}}{2} - v_L + v_{abc}}\right] i_C^2(t) \leq 0 \tag{26}$$

$$i_C(t) \leq 0 \tag{27}$$

Switching criteria for S_3 = off and S_4 = on:

$$v_L(t) - v_{L,max} + \left[\frac{k_A}{\frac{v_{DC}}{2} + v_L - v_{abc}}\right] i_C^2(t) \geq 0 \tag{28}$$

$$i_C(t) \geq 0 \tag{29}$$

$$v_{L,min} = v_L^*(t) - \Delta V \tag{30}$$

$$v_{L,max} = v_L^*(t) + \Delta V \tag{31}$$

Like the regulation of the network's frequency and volage, $v_L^*(t)$ is controlled to achieve the required RMS value. The load reference voltage v_L^* is generated by the PLL from the sinusoidal input voltage v_{abc}. The switch conditions from Equations (26)–(31) determine the gate pulses for the switches. Using feedback signals from the UPQC power circuit, the switching procedures can be carried out while simultaneously satisfying the fluctuations in switching conditions. The production of high-quality voltage at the load is enabled by using the externally assigned reference voltage value as the output.

Thus, UPQC is a versatile device with applications across diverse engineering domains. It addresses PQ issues such as voltage sags, swells, harmonics, and interruptions in

electrical systems, simultaneously regulating both voltage and current to enhance power factor and reduce harmonic distortion. In renewable energy systems, UPQC facilitates the integration of intermittent sources like wind and solar, ensuring a stable power supply. In industrial settings, it protects sensitive equipment by preventing voltage fluctuations, improving overall manufacturing efficiency. UPQC is also integral in smart grids, contributing to stability and reliability amid complex grid structures and the rise of distributed energy resources. Additionally, it plays a crucial role in electric vehicle charging stations, maintaining consistent and high-quality power supply. UPQC's adaptability makes it a valuable tool for improving PQ and reliability in diverse engineering applications.

4. Optimization Problem: Formulation and Algorithm

4.1. Objective Function

Applying a fitness function to fine-tune the gains of the proposed UPQC-FOPID controllers is the objective of the optimization problem. As the minimum of the integral time square error (*ITSE*), represented by *J*, the fitness function is given by:

$$min(J) = min(ITSE) \tag{32}$$

Here, *J* represents the overall error of the presented UPQC controller and the *ITSE* performance index is mathematically represented as:

$$ITSE = \int_0^\infty t^2 |e_t| dt \tag{33}$$

where e_t denotes the error signal. The transfer function C_{FOPID} for the controller is expressed by Equation (34).

$$C_{FOPID}(S) = K_p + \frac{K_i}{S^\lambda} + K_d S^\mu \tag{34}$$

where the FOPID controller variables (K_p, K_i, K_d, λ, and μ), as well as λ and μ, represent the fractional power of integral and differential control, respectively [39]; the contribution signal (i_{abc_ref}) generated by the FOPID control strategy in the dq0 framework to the PWM of the UPQC in the time domain is determined by Equation (35) and can be described as follows:

$$V_{c,dq0} = K_p \, e_{t,dq0} + K_i \, D^{-\lambda} \, e_{t,dq0} + K_d \, D^\mu \, e_{t,dq0} \tag{35}$$

The optimization problem can be subjected to certain non-linear constraints.

4.2. Constraints

The voltage level of the load, denoted as V_L, must fall within a restricted range determined by the minimum and maximum values specified in Equation (36), as follows:

$$0.95 \leq V_L \leq 1.05 \tag{36}$$

The total harmonic distortion of the voltage (THD_v), calculated using Equation (37), should not exceed the maximum value ($THD_{v,max}$) defined in IEEE Standard 519 [27,28], thus

$$THD_v = \frac{\sqrt{\sum_{h=2}^{n} V_h^2}}{V_1} \tag{37}$$

$$THD_v \leq THD_{v,max} \tag{38}$$

4.3. Hybrid Jellyfish Search Optimizer and Particle Swarm Optimizer (HJSPSO)

The HJSPSO algorithm is a hybrid algorithm that combines the merits of the Jellyfish Optimizer (JO) [40] and the Particle Swarm Optimization (PSO) algorithm [41] in exploration of the global solutions. By combining these two methods, the search for a solution

becomes more efficient and effective. By utilizing a time control strategy, the algorithm may switch between the two approaches and obtain the best answer [42]. The parameters used in the hybrid technique strike a balance between exploration and exploitation. In Figure 6, one can see the HJSPSO procedure's flowchart.

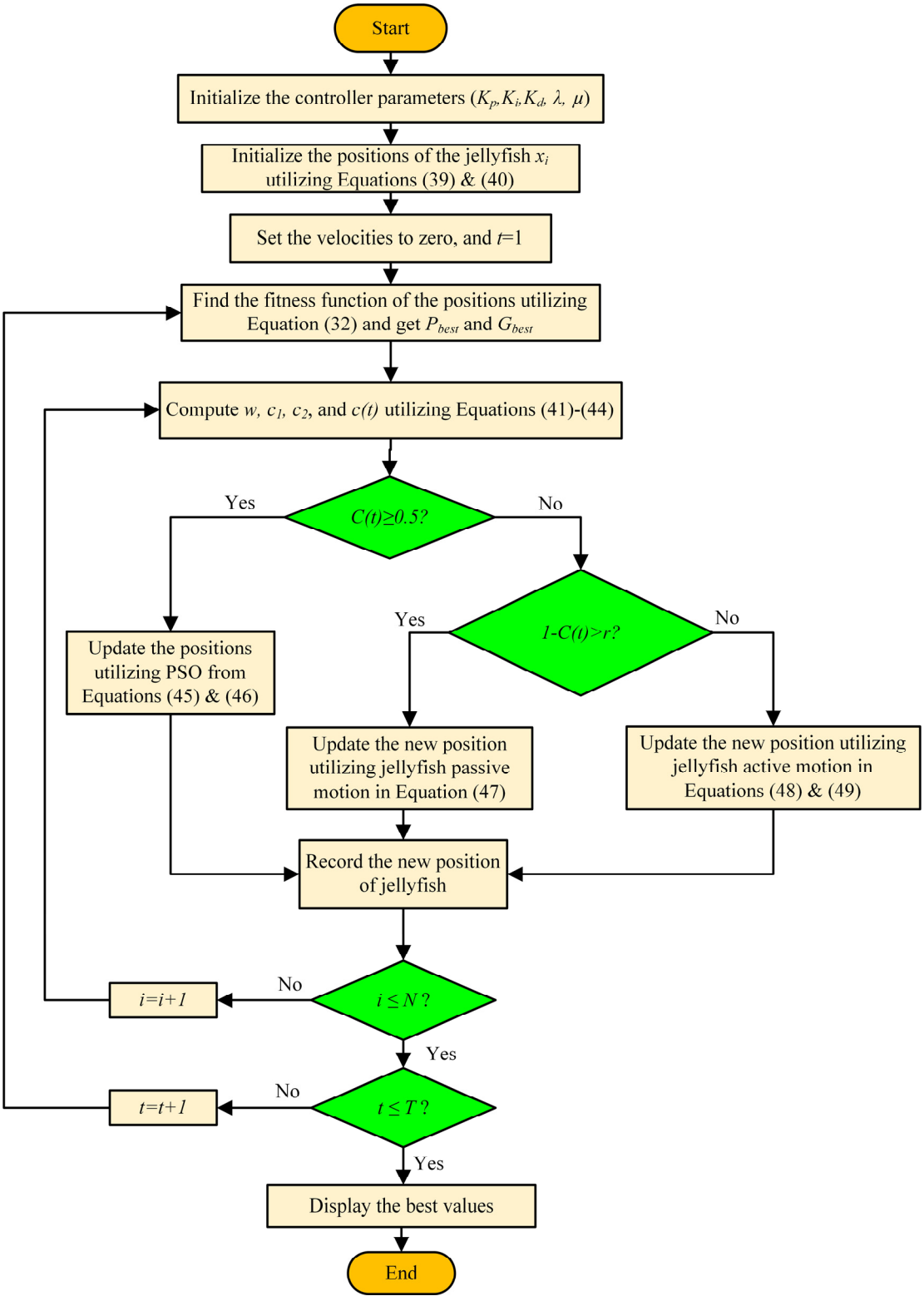

Figure 6. Flowchart of HJSPSO.

For the start of the food search, the HJSPSO algorithm uses the following to initialize the jellyfish positions:

$$X_i = LB + (UB - LB)L_i, \qquad 1 \le i \le N \tag{39}$$

$$L_i^{t+1} = \eta L_i^t \left(1 - L_i^t\right), \qquad 0 < L_i^0 < 1 \tag{40}$$

In the above equations, X_i denotes the current position of the ith jellyfish, LB and UB denote the lower and upper limits of the gains, L_i is the logistic value of the ith jellyfish, L_i^0 is the initial logistic number of the jellyfish, N is the swarm amount, and t is the current iteration. Additionally, η is set to 4. The fitness values are estimated employing the following procedure.

To decide between selecting PSO or JO for upgrading the position, the following equations can be processed:

$$w = w_{min} + (w_{max} - w_{min})\left(1 - \frac{t}{T}\right)^{\beta_1} \tag{41}$$

$$c_1 = c_{min} + (c_{max} - c_{min})\sin\left(\frac{\pi}{2}\left(1 - \frac{t}{T}\right)\right) \tag{42}$$

$$c_2 = c_{min} + (c_{max} - c_{min})\cos\left(\frac{\pi}{2}\left(1 - \frac{t}{T}\right)\right) \tag{43}$$

$$c(t) = \left|\left(1 - \frac{t}{T}\right)(2r - 1)\right| \tag{44}$$

In the above equations, r denotes a random value generated between [0, 1], and T represents the number of iterations performed. If $c(t) \ge 0.5$, PSO is chosen for renovating the position using the following equations:

$$V_i^{t+1} = wV_i^t + c_1 r_1\left(Pbest_i^t - X_i^t\right) + c_2 r_2\left(Gbest^t - X_i^t\right) \tag{45}$$

$$X_i^{t+1} = X_i^t + V_i^{t+1}, \qquad 1 \le i \le N \tag{46}$$

In the above equations, w_{min}, w_{max}, β_1, c_{min}, and c_{max} are set to 0.4, 0.9, 0.1, 0.5, and 2.5, respectively. Additionally, r_1 and r_2 are random values generated in the range [0, 1]. Moreover, V_i denotes the velocity of the ith particle, $Pbest$ represents the optimum personal position, and $Gbest$ represents the global optimum position. Furthermore, the JO can be utilized to renew the position. The JO comprises passive movements (around the current position) and active movements (updating corresponding to a randomly chosen jth jellyfish). The position renovate for these two procedures is stated as follows:

$$X_i^{t+1} = X_i^t + wr_1\left(X^* - 3r_2 X_i^t\right), \qquad 1 \le i \le N, \text{ passive when } (1 - c(t)) > r \tag{47}$$

$$X_i^{t+1} = X_i^t + wr_1\overrightarrow{Step}, \qquad 1 \le i \le N, \text{ active when } (1 - c(t)) < r \tag{48}$$

$$\overrightarrow{Step} = \begin{cases} X_i^t - X_j^t, & if\ f\left(X_i^t\right) < f\left(X_j^t\right) \\ X_j^t - X_i^t, & if\ f\left(X_j^t\right) < f\left(X_i^t\right) \end{cases} \tag{49}$$

where X^* represents the current swarm's best position. The optimum quantities attained utilizing the HJSPSO for FOPID are given in Table 1.

Table 1. Optimum controller factors of the FOPID utilizing the HJSPSO method.

Operating Conditions	FOPID Control Strategy					Time (s)	Objective fn.
	K_p	K_i	K_d	λ	μ		
Sag event	3.541	1.468	0.307	1.6783	0.1523	127.474	1.423
Swell event	3.348	0.476	0.231	1.8441	0.3061	128.846	1.890
3-phase fault	3.304	0.586	0.515	1.6891	0.5704	129.476	1.168
Double line to ground fault	4.051	2.045	0.087	1.6801	0.5690	125.476	1.378

The following section will describe how the fine-tuned parameters of the FOPID controller effectively control the system's performance in different events.

5. Results and Discussions

5.1. Power Quality Issues

5.1.1. Event #1: Balanced Sag

In a three-phase balanced sag, when specific heavy loads can be switched off in each of the three phases, a sag mode occurs. Therefore, it was decided to utilize the sag mode for the test conducted between t = 0.15 and t = 0.25 s. The simulation findings explain the voltage at the V_L bus for each of the three phases through this circumstance. Figure 7 depicts the load voltage before and after connecting the FOPID-UPQC to the system. The presence of harmonics in a system generated by the sag event is shown in Figure 8 by the study of the *THD*. The *THD* values of the load voltage (V_L) in the suggested controller-based approach are 6.31% and 1.74%, respectively.

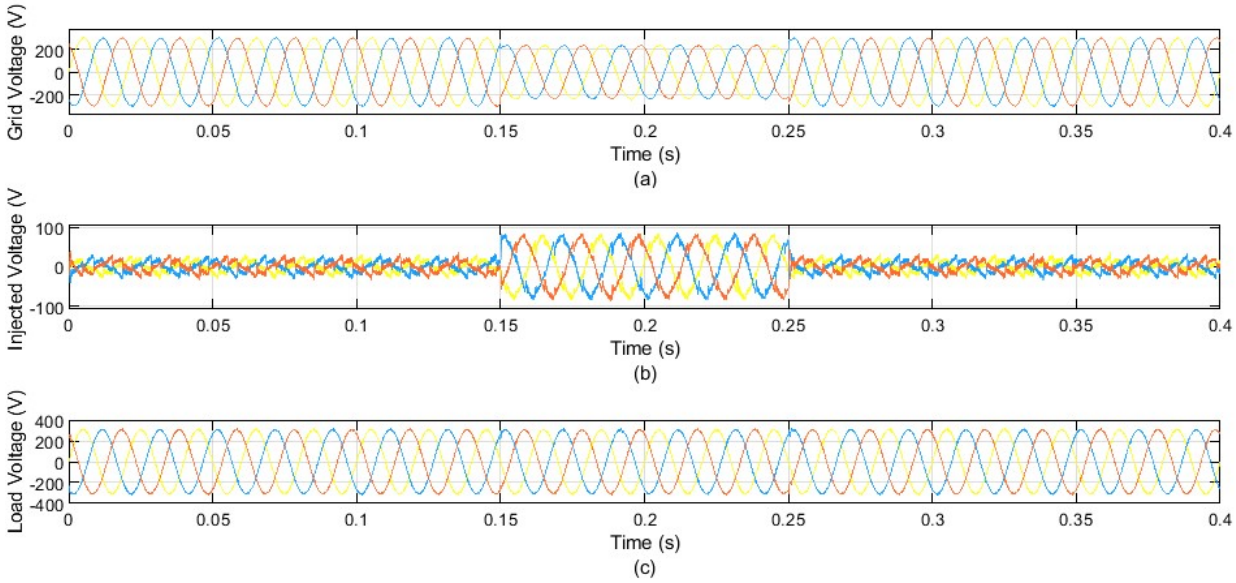

Figure 7. The simulated outcomes for the sag mode using the UPQC: (**a**) the network voltage without enhancement, (**b**) the injected voltage, and (**c**) the load voltage with enhancement.

5.1.2. Event #2: Balanced Swell

The three-phase balanced swell occurs when different heavy loads are turned off. For that reason, it seemed probable that the swell mode would be applied during the test from t = 0.15 s to t = 0.25 s. Each of the three phases' voltage at the V_L is depicted in the simulation results for this event. Figure 9 illustrates the load voltage with and without enhancement utilizing the FOPID-UPQC.

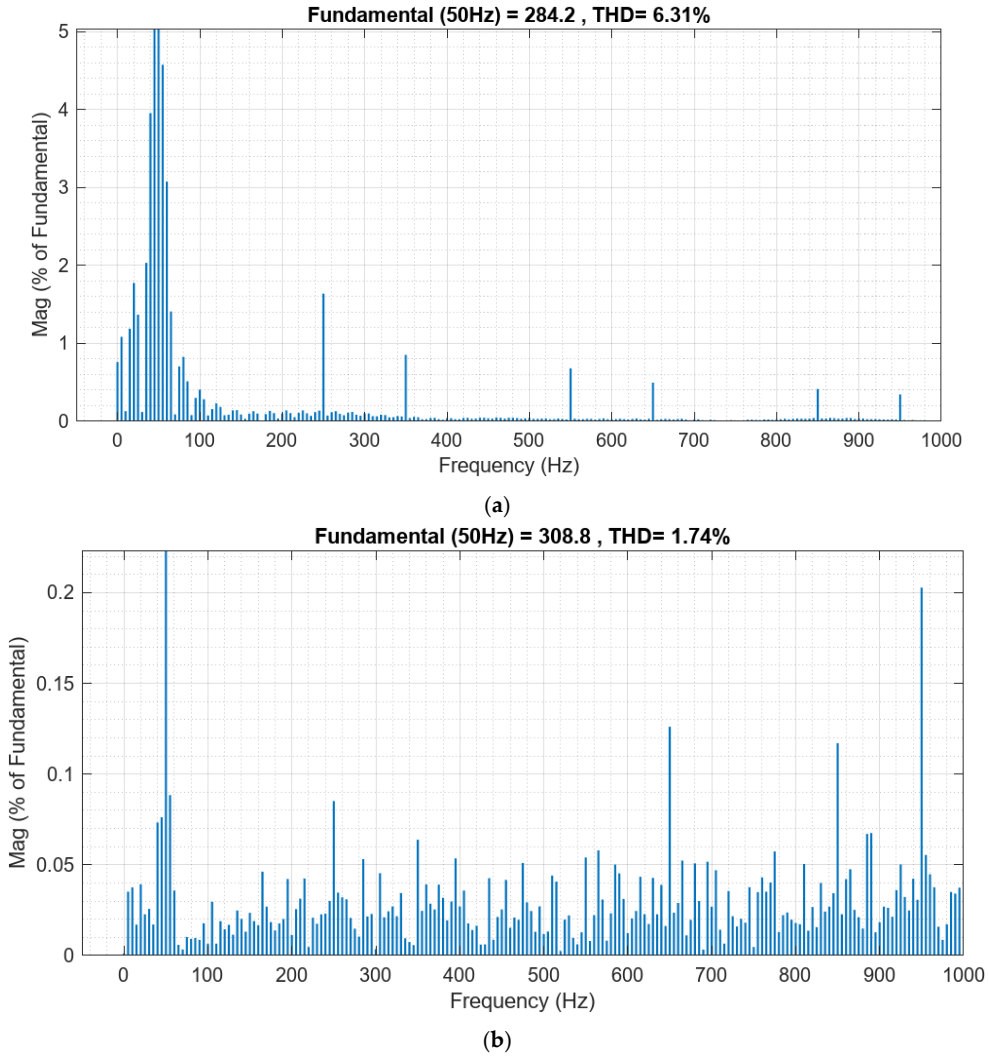

Figure 8. THD_v analysis in voltage: (**a**) before enhancement, and (**b**) after enhancement in sag condition.

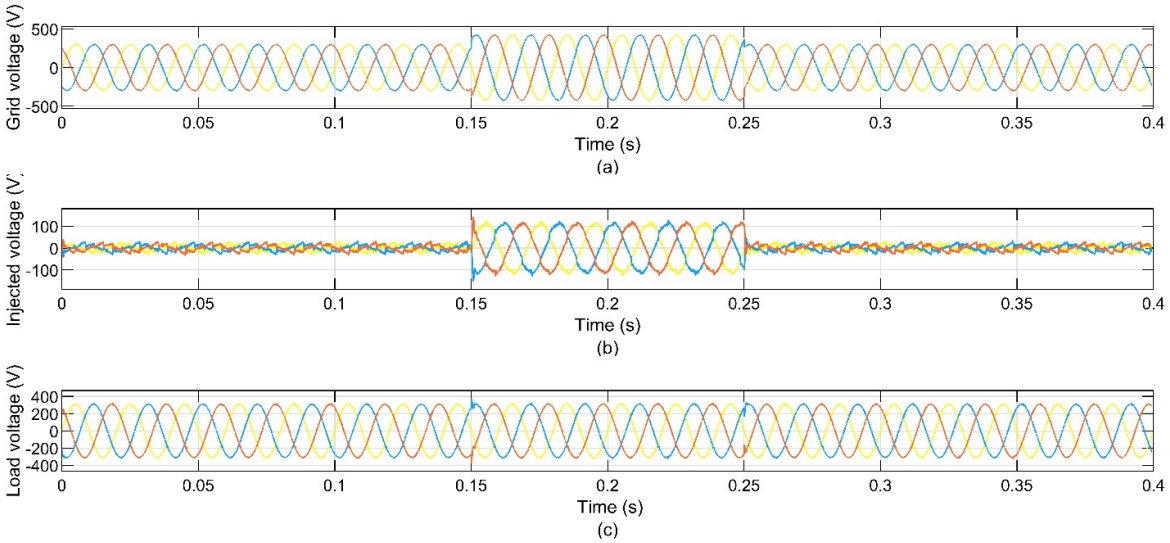

Figure 9. The simulated outcomes for the swell mode using the UPQC: (**a**) the network voltage without enhancement, (**b**) the injected voltage, and (**c**) the load voltage with compensation.

As shown in Figure 10, a look at the *THD* indicates the presence of harmonics in a system generated by a swell event [43]. With no enhancement, the V_L's *THD* value in the suggested controller-based model is 10.70%, while with enhancement, it is 1.68%.

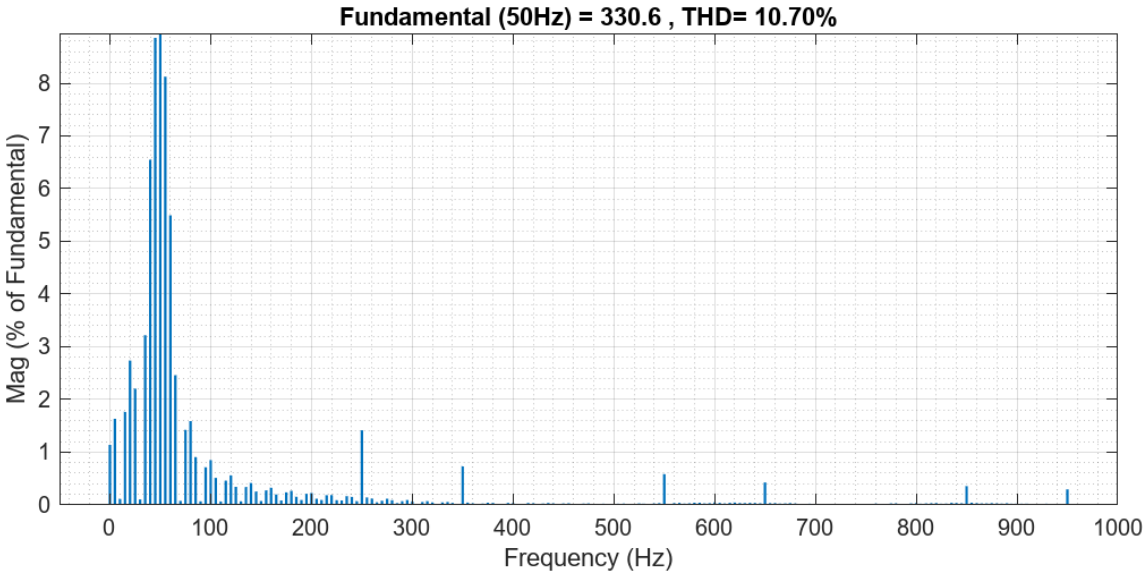

(**a**)

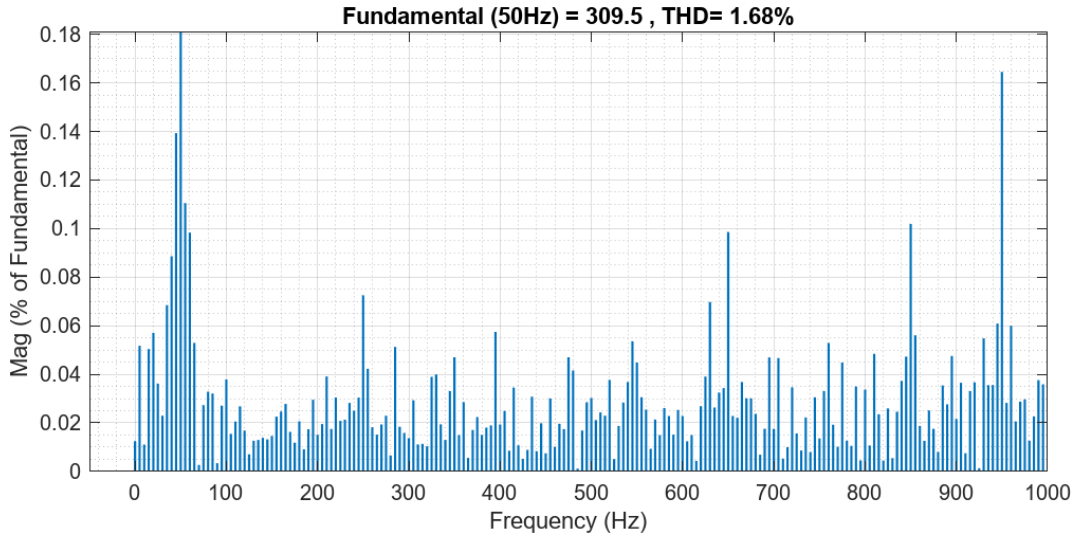

(**b**)

Figure 10. THD_v analysis: (**a**) before enhancement, and (**b**) after enhancement under swell condition.

5.1.3. Event #3: Three-Phase Faults

Three-phase faults, which are a PQ concern, impact the components on the load side of the system. Figure 11 depicts the interruption status along with the injected current and voltage, as well as the load voltage. The figure illustrates that the interruption occurs, interrupting the power flow for a period of 0.15 to 0.25 s, as determined by the controller. Figure 12 presents the analysis of the *THD*, which represents the presence of harmonics in a system caused by interruption condition. In the proposed controller-based model, the *THD* values of the V_L with and without enhancement are 7.76% and 1.74%, respectively.

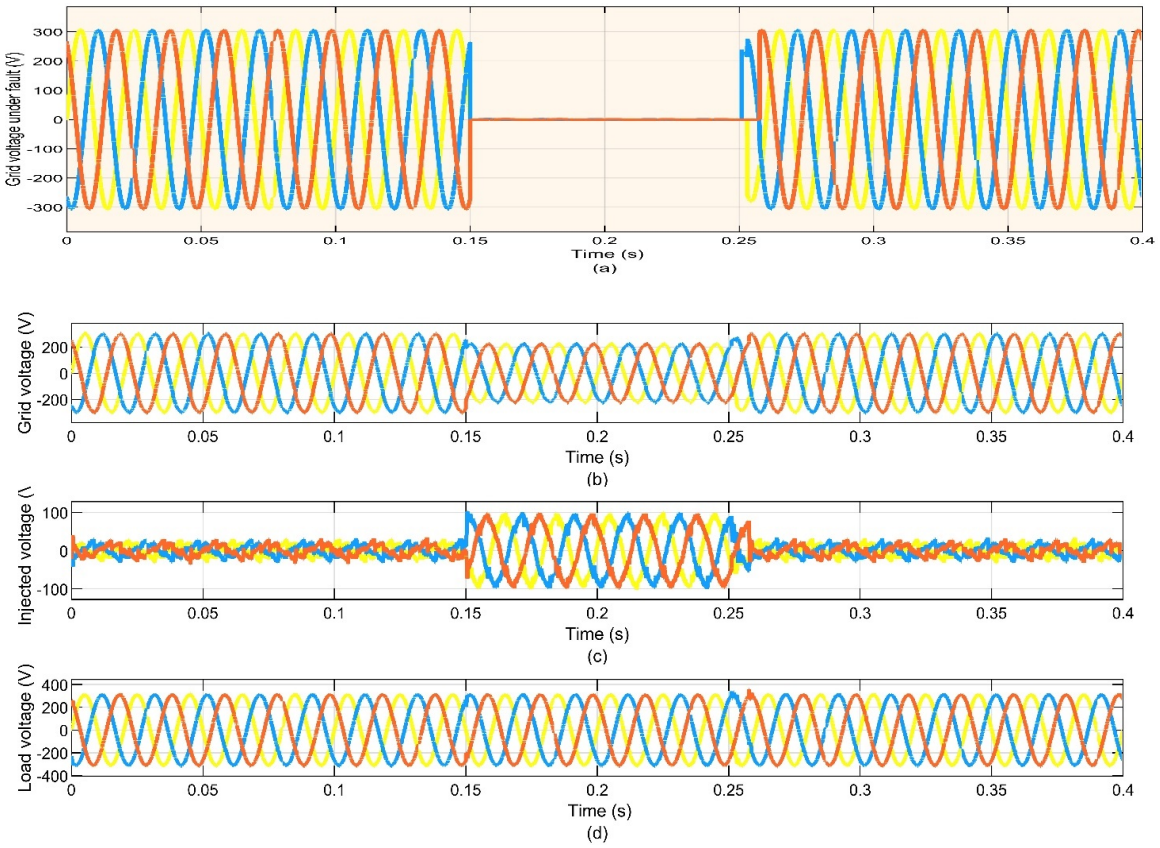

Figure 11. The simulated results for a three-phase faults mode using the UPQC: (**a**) the second feeder voltage during fault, (**b**) the network voltage without compensation, (**c**) the injected voltage, and (**d**) the load voltage with compensation.

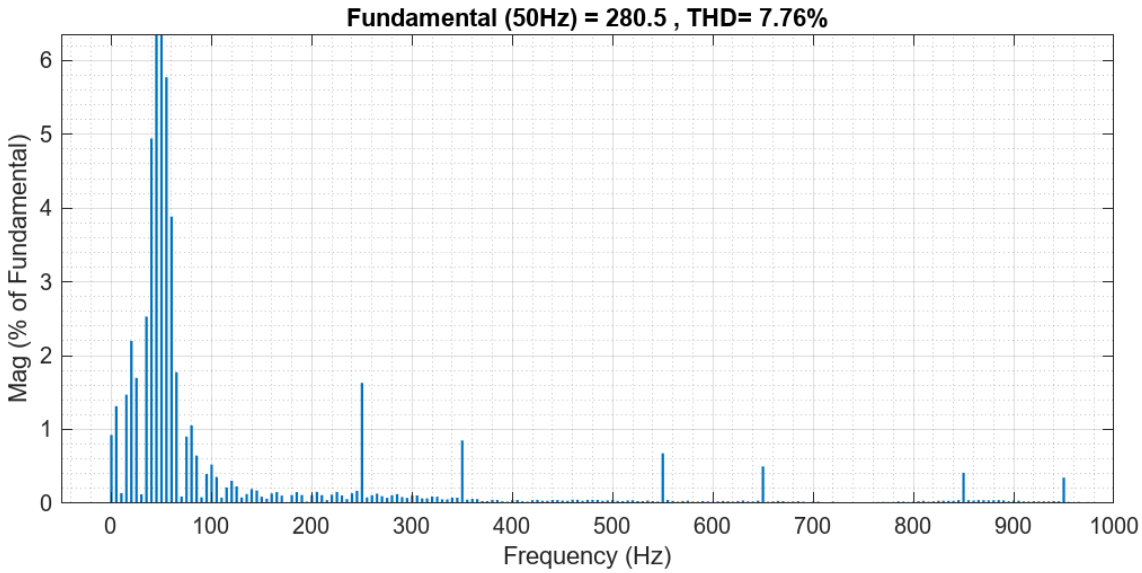

(**a**)

Figure 12. *Cont.*

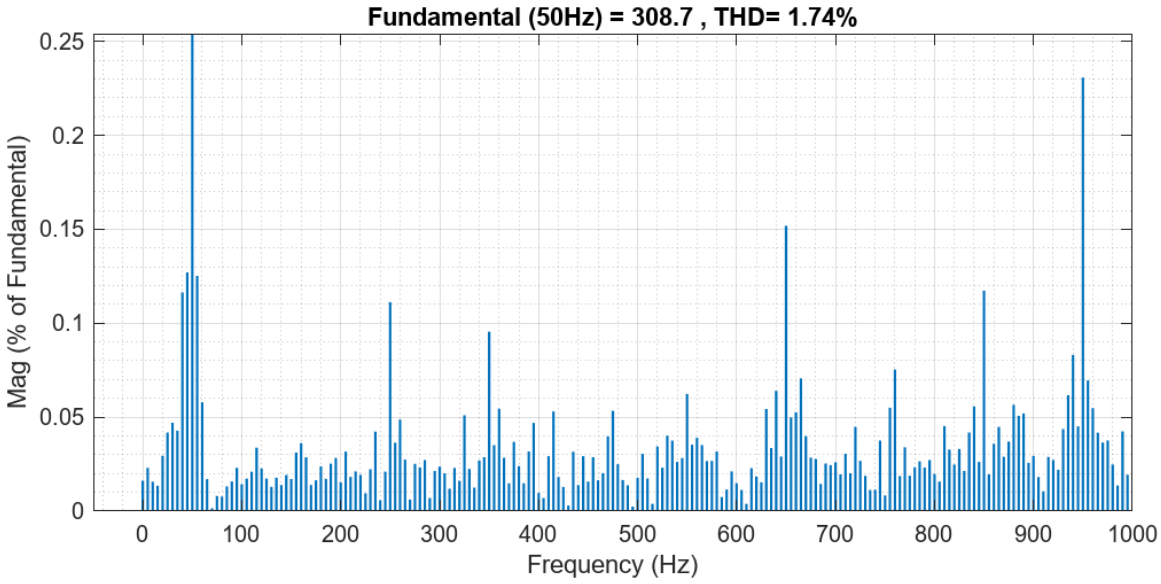

(**b**)

Figure 12. THD_v analysis in voltage: (**a**) before enhancement, and (**b**) after enhancement in the interruption condition.

5.1.4. Event #4: Double Line to Ground

Between t = 0.15 s and t = 0.25 s, a double line to ground fault arises at the first feeder, specifically between phase A and B. In response to this fault, the controller swiftly injects the necessary voltage. Figure 13 illustrates the voltage before and after enhancement, along with the injected voltage.

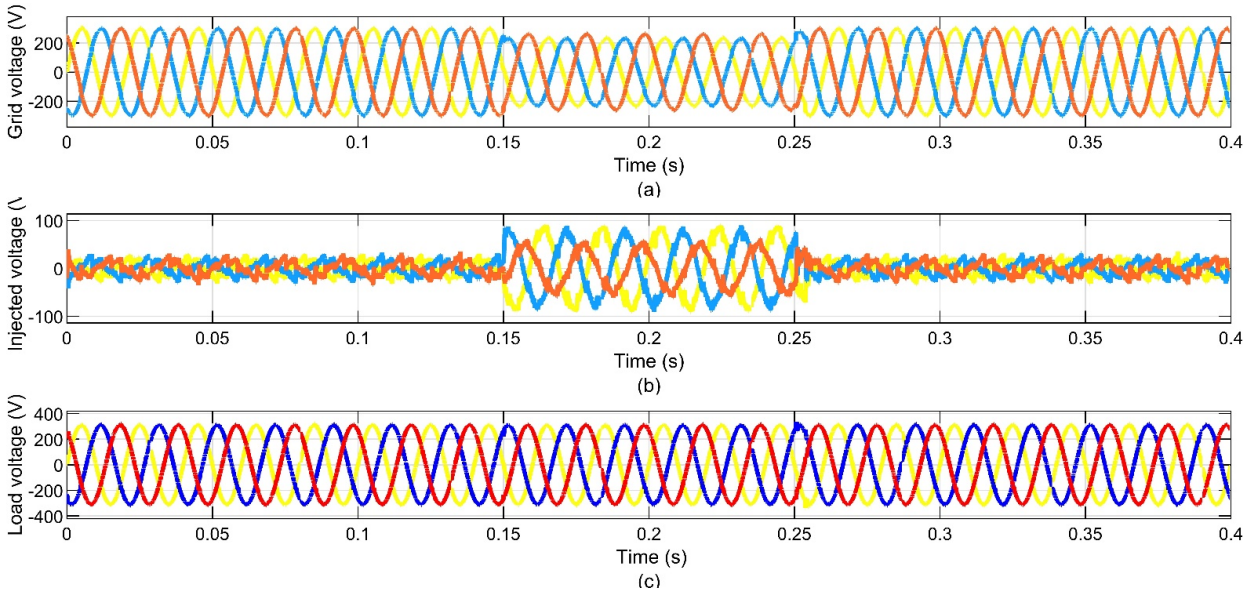

Figure 13. The simulated outcomes for the double line to ground (DLG) mode using the UPQC: (**a**) the grid voltage without compensation, (**b**) the injected voltage, and (**c**) the load voltage with compensation.

Figure 14 presents the analysis of the *THD*, which represents the presence of harmonics in the system in the DLG condition. Using the proposed controller-based model, the *THD* values of the voltage before and after enhancement are 7.14% and 1.73%, respectively.

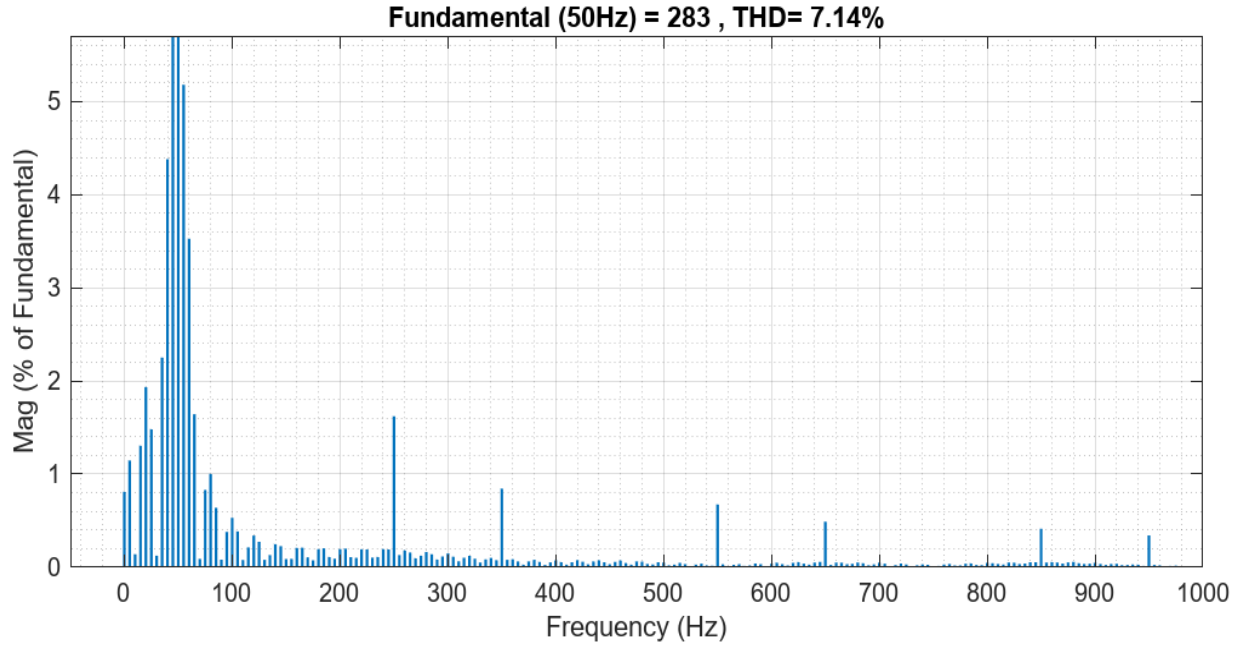

(**a**)

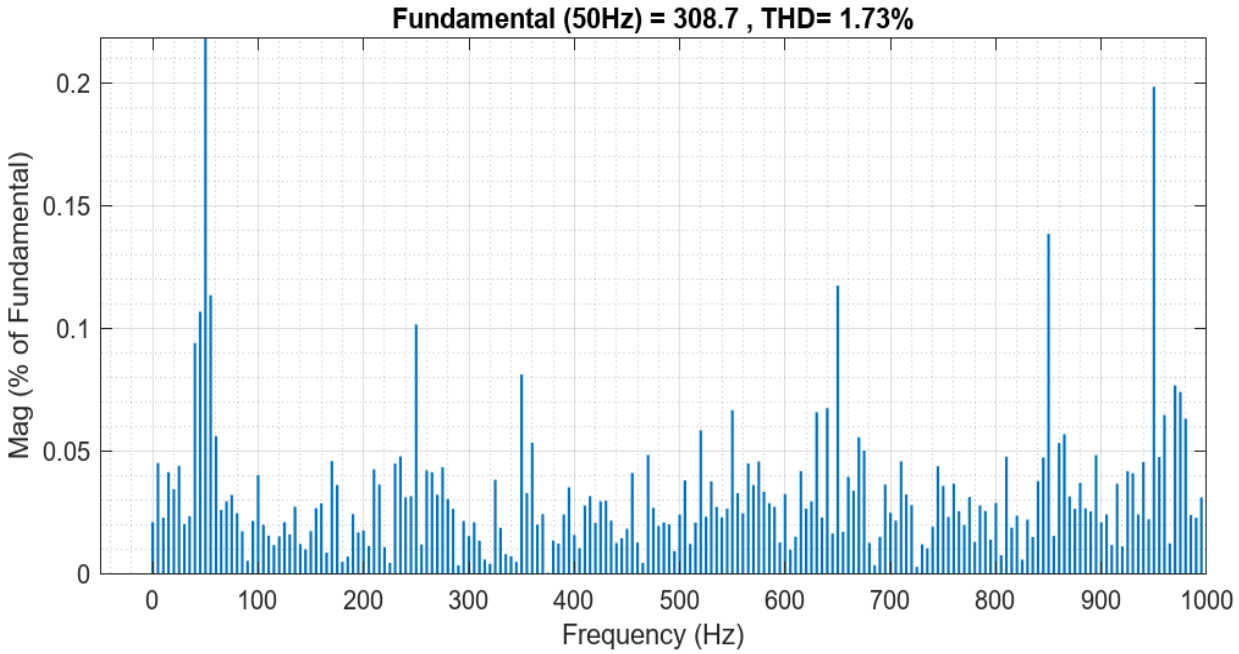

(**b**)

Figure 14. *THDv* analysis: (**a**) before enhancement, and (**b**) after enhancement in DLG condition.

5.2. Comparative Investigation

To improve the UPQC scheme's robustness, this section presents two comparison studies that evaluate several optimization approaches and an alternative controller.

5.2.1. Comparison of HJSPSO and Other Optimization Methods

The performance of various optimization strategies, such as the Grasshopper Optimization Algorithm (GOA) [12], the Salp Swarm Algorithm (SSA), and the proposed HJSPSO approach, is evaluated to simulate the tuning of the presented UPQC scheme. Table 2 illustrates the differences between these three methods, which are in line with the objective. Results show the HJSPSO effectiveness. Figure 15 depicts the GOA, SSA, and

HJSPSO convergence curves. According to the results, HJSPSO always finds the best values for the objective function with the fewest iterations.

Table 2. A comparative analysis of numerous FOPID controllers' optimization approaches.

Optimization Methods	GOA	SSA	HJSPSO
Max. iteration	250	250	250
Number of search agents	100	100	100
Computing time (s)	159.544	212.405	127.474
Objective function	1.747	1.987	1.423
K_p	2.261	3.766	3.541
K_i	1.991	1.898	1.468
K_d	0.541	0.468	0.307
λ	1.4786	1.7894	1.6783
μ	0.2487	0.1479	0.1523

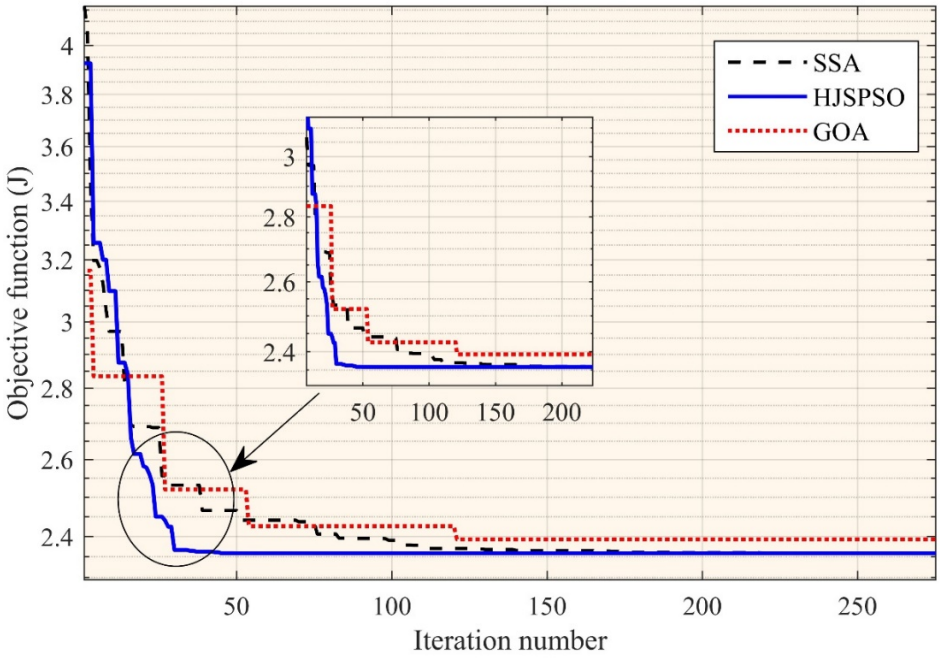

Figure 15. Convergence rates in the sag event.

5.2.2. Comparative Evaluation of Two Different Controllers

A comparison was conducted between the UPQC-FOPID performance and another controller known as the fuzzy logic controller (FLC) to assess their effectiveness and robustness. To handle balanced swells, sags, and other fault conditions, the suggested model was tested on the MATLAB/Simulink platform. In Table 3, the results and comparative analysis between the presented UPQC-FOPID controller and the UPQC-FLC typology under diverse grid conditions like voltage sag, swell, and fault circumstances are displayed and evaluated. The obtained findings demonstrate the superiority of the UPQC-FOPID control strategy according to its fast response and minimal fitness.

Table 3. The findings with UPQC-FLC and presented UPQC-FOPID.

Scenarios	Computing Time (s)		Comparative Index (J)	
	UPQC-FLC	**UPQC-FOPID**	**UPQC-FLC**	**UPQC-FOPID**
Event #1: Balanced sag	187.474	127.474	2.831	1.423
Event #2: Balanced swell	188.011	128.846	2.092	1.890
Event #3: 3-phase fault	158.505	129.476	2.038	1.168
Event #4: Double line to ground fault	204.112	125.476	2.478	1.378

6. Conclusions

In this study, a novel hybrid RES was introduced. The system consisted of PV-wind farms capable of accommodating non-linear loads. To address PQ issues commonly associated with RESs, such as voltage sag, swell, and harmonics, a UPQC was utilized. The control of UPQC was achieved by employing a FOPID controller with the HJSPSO, which allowed for determining optimal gain values across various PQ issues.

Two comparative investigations were included in the study. The first step was to evaluate the provided HJSPSO optimization approach against two optimization techniques. The results showed that compared to previous optimization approaches, the suggested HJSPSO strategy significantly outperformed them, with the shortest computing time of 127.474 s and an objective function value of 1.423. Second, under various conditions, such as voltage swells, sags, and fault scenarios, the proposed FOPID controller was compared to another controller known as the FLC. The results showed that the UPQC-FOPID controller was superior to the FLC thanks to its quick response and low objective function values. Results showed that the suggested control method worked well when subjected to changes in network voltage in terms of both voltage response and harmonic reduction.

Last but not least, PQ conditioners and harmonics management are critical components in modern power systems, addressing issues related to unwanted frequencies. These unwanted frequencies can compromise system stability, reduce equipment reliability, and lead to energy inefficiencies. PQ conditioners play a pivotal role in mitigating harmonics, ensuring a clean power supply that promotes stability and reliability, particularly with the growing use of electric vehicles and RES. By preventing voltage distortion, avoiding energy losses, and safeguarding sensitive electronic devices, these systems contribute to improved efficiency, reduced operational costs, and compliance with industry standards. In essence, their presence is essential for maintaining a consistent, reliable, and efficient power supply, ultimately preventing downtime and protecting the longevity of electrical equipment in diverse applications.

Finally, suggestions for future works are to conduct further experimental validation in a larger-scale power system setup or in a real-world distribution system to evaluate the performance of the proposed approach under more realistic operating conditions. This will provide valuable insights into the scalability and effectiveness of the proposed approach in practical applications.

Funding: This study is supported via funding from Prince Sattam bin Abdulaziz University, project number (PSAU/2024/R/1445).

Data Availability Statement: The data presented in this study are available on request from the corresponding author. The data are not publicly available due to their large size.

Acknowledgments: The author acknowledges Prince Sattam bin Abdulaziz University, project number (PSAU/2024/R/1445), for their technical and financial support.

Conflicts of Interest: The author declares no conflicts of interest.

References

1. Hirsch, A.; Parag, Y.; Guerrero, J. Microgrids: A Review of Technologies, Key Drivers, and Outstanding Issues. *Renew. Sustain. Energy Rev.* **2018**, *90*, 402–411. [CrossRef]
2. Hernández-Mayoral, E.; Madrigal-Martínez, M.; Mina-Antonio, J.D.; Iracheta-Cortez, R.; Enríquez-Santiago, J.A.; Rodríguez-Rivera, O.; Martínez-Reyes, G.; Mendoza-Santos, E. A Comprehensive Review on Power-Quality Issues, Optimization Techniques, and Control Strategies of Microgrid Based on Renewable Energy Sources. *Sustainability* **2023**, *15*, 9847. [CrossRef]
3. Golla, M.; Sankar, S.; Chandrasekaran, K. Renewable Integrated UAPF Fed Microgrid System for Power Quality Enhancement and Effective Power Flow Management. *Int. J. Electr. Power Energy Syst.* **2021**, *133*, 107301. [CrossRef]
4. Aganović, M.L.; Konjić, T.; Milovanović, M.; Ćalasan, M.; Omar, A.I.; Abdel Aleem, S.H.E. Power Quality in Modern Power Systems: A Case Study in Bosnia and Herzegovina. In *Modernization of Electric Power Systems: Energy Efficiency and Power Quality*; Zobaa, A.F., Abdel Aleem, S.H.E., Eds.; Springer International Publishing: Cham, Switzerland, 2023; pp. 181–204. ISBN 9783031189968.
5. Ravi, T.R.; Kumar, K.S.; Dhanamjayulu, C.; Khan, B.; Rajalakshmi, K. Analysis and Mitigation of PQ Disturbances in Grid Connected System Using Fuzzy Logic Based IUPQC. *Sci. Rep.* **2023**, *13*, 22425. [CrossRef]
6. Alhaiz, H.A.; Alsafran, A.S.; Almarhoon, A.H. Single-Phase Microgrid Power Quality Enhancement Strategies: A Comprehensive Review. *Energies* **2023**, *16*, 5576. [CrossRef]
7. Oubrahim, Z.; Amirat, Y.; Benbouzid, M.; Ouassaid, M. Power Quality Disturbances Characterization Using Signal Processing and Pattern Recognition Techniques: A Comprehensive Review. *Energies* **2023**, *16*, 2685. [CrossRef]
8. Jha, K.; Shaik, A.G. A Comprehensive Review of Power Quality Mitigation in the Scenario of Solar PV Integration into Utility Grid. *e-Prime Adv. Electr. Eng. Electron. Energy* **2023**, *3*, 100103. [CrossRef]
9. Bajaj, M.; Singh, A.K. Grid Integrated Renewable DG Systems: A Review of Power Quality Challenges and State-of-the-Art Mitigation Techniques. *Int. J. Energy Res.* **2020**, *44*, 26–69. [CrossRef]
10. Shafiullah, M.; Ahmed, S.D.; Al-Sulaiman, F.A. Grid Integration Challenges and Solution Strategies for Solar PV Systems: A Review. *IEEE Access* **2022**, *10*, 52233–52257. [CrossRef]
11. Ibrahim, N.F.; Mahmoud, M.M.; Al Thaiban, A.M.; Barnawi, A.B.; Elbarbary, Z.S.; Omar, A.I.; Abdelfattah, H. Operation of Grid-Connected PV System with ANN-Based MPPT and an Optimized LCL Filter Using GRG Algorithm for Enhanced Power Quality. *IEEE Access* **2023**, *11*, 106859–106876. [CrossRef]
12. Omar, A.I.; Abdel Aleem, S.H.E.; El-Zahab, E.E.A.; Algablawy, M.; Ali, Z.M. An Improved Approach for Robust Control of Dynamic Voltage Restorer and Power Quality Enhancement Using Grasshopper Optimization Algorithm. *ISA Trans.* **2019**, *95*, 110–129. [CrossRef]
13. Elmetwaly, A.H.; ElDesouky, A.A.; Omar, A.I.; Attya Saad, M. Operation Control, Energy Management, and Power Quality Enhancement for a Cluster of Isolated Microgrids. *Ain Shams Eng. J.* **2022**, *13*, 101737. [CrossRef]
14. Mahmoud, M.M.; Atia, B.S.; Esmail, Y.M.; Ardjoun, S.A.E.M.; Anwer, N.; Omar, A.I.; Alsaif, F.; Alsulamy, S.; Mohamed, S.A. Application of Whale Optimization Algorithm Based FOPI Controllers for STATCOM and UPQC to Mitigate Harmonics and Voltage Instability in Modern Distribution Power Grids. *Axioms* **2023**, *12*, 420. [CrossRef]
15. Sepasi, S.; Talichet, C.; Pramanik, A.S. Power Quality in Microgrids: A Critical Review of Fundamentals, Standards, and Case Studies. *IEEE Access* **2023**, *11*, 108493–108531. [CrossRef]
16. Amini, M.A.; Jalilian, A. Modelling and Improvement of Open-UPQC Performance in Voltage Sag Compensation by Contribution of Shunt Units. *Electr. Power Syst. Res.* **2020**, *187*, 106506. [CrossRef]
17. B, S.G. BWO Strategy for Power Quality Improvement in HRES Grid-Connected DPFC System. *Smart Sci.* **2021**, *9*, 226–243. [CrossRef]
18. Bharat Mohan, N.; Rajagopal, B.; Hari Krishna, D. Power Quality Enhancement of Hybrid Renewable Energy Source-Based Distribution System Using Optimised UPQC. *J. Control Decis.* **2023**, 1–22. [CrossRef]
19. Rao, B.S.; Kumar, D.V.; Kumar, K.K. Power Quality Improvement Using Cuckoo Search Based Multilevel Facts Controller. *J. Eng. Res.* **2022**, *10*, 252–261. [CrossRef]
20. Krishna, D.; Sasikala, M.; Kiranmayi, R. FOPI and FOFL Controller Based UPQC for Mitigation of Power Quality Problems in Distribution Power System. *J. Electr. Eng. Technol.* **2022**, *17*, 1543–1554. [CrossRef]
21. Samal, S.; Hota, P.K. Wind Energy Fed Upqc System for Power Quality Improvement. *Bull. Electr. Eng. Inform.* **2018**, *7*, 495–504. [CrossRef]
22. Nafeh, A.A.; Heikal, A.; El-Sehiemy, R.A.; Salem, W.A.A. Intelligent Fuzzy-Based Controllers for Voltage Stability Enhancement of AC-DC Micro-Grid with D-STATCOM. *Alex. Eng. J.* **2021**, *61*, 2260–2293. [CrossRef]
23. Elmetwaly, A.H.; Younis, R.A.; Abdelsalam, A.A.; Omar, A.I.; Mahmoud, M.M.; Alsaif, F.; El-Shahat, A.; Saad, M.A. Modeling, Simulation, and Experimental Validation of a Novel MPPT for Hybrid Renewable Sources Integrated with UPQC: An Application of Jellyfish Search Optimizer. *Sustainability* **2023**, *15*, 5209. [CrossRef]
24. Dheeban, S.S.; Muthu Selvan, N.B. ANFIS-Based Power Quality Improvement by Photovoltaic Integrated UPQC at Distribution System. *IETE J. Res.* **2023**, *69*, 2353–2371. [CrossRef]
25. Das, S.R.; Ray, P.K.; Sahoo, A.K.; Ramasubbareddy, S.; Babu, T.S.; Kumar, N.M.; Elavarasan, R.M.; Mihet-Popa, L. A Comprehensive Survey on Different Control Strategies and Applications of Active Power Filters for Power Quality Improvement. *Energies* **2021**, *14*, 4589. [CrossRef]

26. Abdel Mohsen, S.E.; Ibrahim, A.M.; Elbarbary, Z.M.S.; Omar, A.I. Unified Power Quality Conditioner Using Recent Optimization Technique: A Case Study in Cairo Airport, Egypt. *Sustainability* **2023**, *15*, 3710. [CrossRef]
27. Mosaad, M.I.; Abed El-Raouf, M.O.; Al-Ahmar, M.A.; Bendary, F.M. Optimal PI Controller of DVR to Enhance the Performance of Hybrid Power System Feeding a Remote Area in Egypt. *Sustain. Cities Soc.* **2019**, *47*, 101469. [CrossRef]
28. Monteiro, V.; Moreira, C.; Pecas Lopes, J.A.; Antunes, C.H.; Osório, G.J.; Catalão, J.P.S.; Afonso, J.L. A Novel Three-Phase Multiobjective Unified Power Quality Conditioner. *IEEE Trans. Ind. Electron.* **2024**, *71*, 59–70. [CrossRef]
29. Gade, S.; Agrawal, R. Optimal Utilization of Unified Power Quality Conditioner Using the JAYA Optimization Algorithm. *Eng. Optim.* **2023**, *55*, 1–18. [CrossRef]
30. Sai Sarita, N.C.; Suresh Reddy, S.; Sujatha, P. Control Strategies for Power Quality Enrichment in Distribution Network Using UPQC. *Mater. Today Proc.* **2023**, *80*, 2872–2882. [CrossRef]
31. Omar, A.I.; Mohsen, M.; Abd-Allah, M.A.; Salem Elbarbary, Z.M.; Said, A. Induced Overvoltage Caused by Indirect Lightning Strikes in Large Photovoltaic Power Plants and Effective Attenuation Techniques. *IEEE Access* **2022**, *10*, 112934–112947. [CrossRef]
32. Said, A.; Abd-Allah, M.A.; Mohsen, M.; Omar, A.I. Alleviation of the Transients Induced in Large Photovoltaic Power Plants by Direct Lightning Stroke. *Ain Shams Eng. J.* **2022**, *14*, 101880. [CrossRef]
33. Awad, M.; Mahmoud, M.M.; Elbarbary, Z.M.S.; Ali, L.M.; Fahmy, S.N.; Omar, A.I. Design and Analysis of Photovoltaic/Wind Operations at MPPT for Hydrogen Production Using a PEM Electrolyzer: Towards Innovations in Green Technology. *PLoS ONE* **2023**, *18*, e0287772. [CrossRef]
34. Boudjemai, H.; Ardjoun, S.A.E.M.; Chafouk, H.; Denai, M.; Elbarbary, Z.M.S.; Omar, A.I.; Mahmoud, M.M. Application of a Novel Synergetic Control for Optimal Power Extraction of a Small-Scale Wind Generation System with Variable Loads and Wind Speeds. *Symmetry* **2023**, *15*, 369. [CrossRef]
35. Shi, S.; Liu, D.; Han, J. Small Signal Modeling and Performance Analysis of Conventional- and Dual-UPQC. *IEEE Access* **2024**, *12*, 11909–11925. [CrossRef]
36. Amirullah, A.; Adiananda, A. Dual Fuzzy-Sugeno Method to Enhance Power Quality Performance Using a Single-Phase Dual UPQC-Dual PV without DC-Link Capacitor. *Prot. Control Mod. Power Syst.* **2024**, *9*, 133–153. [CrossRef]
37. Srilakshmi, K.; Rao, G.S.; Swarnasri, K.; Inkollu, S.R.; Kondreddi, K.; Balachandran, P.K.; Colak, I. Optimization of ANFIS Controller for Solar/Battery Sources Fed UPQC Using an Hybrid Algorithm. *Electr. Eng.* **2024**. [CrossRef]
38. Sanjenbam, C.D.; Singh, B. Power Quality Enhancement of Standalone Hydropower Generation System through Modified Integrator Based Observer Controlled UPQC. *Electr. Power Syst. Res.* **2024**, *226*, 109941. [CrossRef]
39. Rawa, M.; Alghamdi, S.; Calasan, M.; Aldosari, O.; Ali, Z.M.; Alkhalaf, S.; Micev, M.; Abdel Aleem, S.H.E. Disturbance Rejection-Based Optimal PID Controllers for New 6ISO AVR Systems. *Fractal Fract.* **2023**, *7*, 765. [CrossRef]
40. Chou, J.S.; Truong, D.N. A Novel Metaheuristic Optimizer Inspired by Behavior of Jellyfish in Ocean. *Appl. Math. Comput.* **2021**, *389*, 125535. [CrossRef]
41. Slowik, A. Particle Swarm Optimization. In *Proceedings of the The Industrial Electronics Handbook—Five Volume Set*; IEEE: Piscataway, NJ, USA, 2011; Volume 4, pp. 1942–1948.
42. Zobaa, A.F.; Aleem, S.H.E.A.; Abdelaziz, A.Y. *Classical and Recent Aspects of Power System Optimization*; Elsevier: Amsterdam, The Netherlands, 2018; ISBN 9780128124420.
43. Zobaa, A.F.; Abdel Aziz, M.M.; Abdel Aleem, S.H.E. Comparison of Shunt-Passive and Series-Passive Filters for DC Drive Loads. *Electr. Power Compon. Syst.* **2010**, *38*, 275–291. [CrossRef]